

Study on Superconducting Properties of Heavy-Fermion CeIrIn₅ Thin Films

grown via Pulsed Laser Deposition

Ji-Hoon Kang, Jihyun Kim, Woo Seok Choi,

Sungmin Park*, and Tuson Park**

Department of Physics, Sungkyunkwan University, Suwon, 16419, Republic of Korea

ABSTRACT

Herein, we report CeIrIn₅ thin-film growth on a MgF₂ (001) substrate using pulsed laser deposition technique. X-ray diffraction analysis showed that the thin films were either mainly *a*-axis-oriented (TF1) or a combination of *a*- and *c*-axis-oriented (TF2). The characteristic features of Kondo coherence temperature (T_{coh}) and superconductivity (T_c) were clearly observed, where onset of T_c is 0.58 and 0.52 K, and $T_{\text{coh}} = 41$ K and 37 K for TF1 and TF2, respectively. The temperature dependencies of the upper critical field (H_{c2}) of both thin films and the bulk CeIrIn₅ single crystal revealed a scaling behavior, indicating that the nature of unconventional superconductivity has not been changed in the thin film. The successful synthesis of CeIrIn₅ thin films is expected to open a new avenue for novel quantum phases that may have been difficult to explore in the bulk crystalline samples.

Keywords: CeIrIn₅ thin film, heavy fermions, superconductivity, metal thin film, pulsed laser deposition

*Corresponding author. E-mail: tp8701@skku.edu, imsuper007@gmail.com

I. INTRODUCTION

Heavy-fermion compounds have attracted great interest because of their various novel properties, such as unconventional superconductivity, quantum criticality, and non-Fermi liquid behavior [1-3]. In strongly correlated electron systems with partially occupied f orbitals, localized moments are hybridized with itinerant electrons, producing an entangled quantum state with a heavy effective mass [4]. The prototypical family, CeMIn_5 ($M = \text{Rh, Co, or Ir}$), exhibits various quantum critical phenomena that can be controlled via nonthermal parameters such as pressure, doping, or magnetic fields with relative ease because their characteristic energy scales are meV range [1, 5, 6]. Recently, dimensional tuning of CeMIn_5 via molecular beam epitaxy (MBE) has been successfully performed to produce superlattice structures such as $\text{CeCoIn}_5(n)/\text{YbCoIn}_5(5)$ (with n being the number of the layer) and $\text{CeCoIn}_5(5)/\text{CeRhIn}_5(5)$, opening a new opportunity to systematically control the novel phases of heavy-fermion systems in the reduced spatial dimension [7, 8].

CeIrIn_5 , which crystallizes in a tetragonal structure, reaches the zero-resistance superconducting (SC) state at 1.2 K ($= T_c$) under ambient pressure [9]. However, thermodynamic studies that measured bulk properties revealed a bulk superconducting phase transition at 0.4 K, raising a question on the nature of the high- T_c phase [10-11]. Recently, spatially varying superconducting domains were reported in single-crystal CeIrIn_5 that was cut into a tiny lamella and attached to an Al_2O_3 substrate [12]. Depending on the orientation of the transport measurements, T_c varies from 200 mK to 1.2 K, suggesting that the T_c difference between the transport and bulk measurements is induced from the defect-strained superconducting patches. Complex strain fields in the single crystal, which were introduced by focused ion beam (FIB) patterning, were argued as the origin of the heterogeneous electronic phases, making strain as a promising nonthermal tuning parameter of unconventional superconductivity. However, since FIB technique is not easily accessible on a bulk

single crystal, thin film growth could be a more effective route for strain engineering, which is expected to deepen our understanding on the origin of the high- T_c phase in CeIrIn₅ and other quantum phenomena that could be amplified in the reduced spatial dimension [13].

In this Letter, we report the synthesis of heavy-fermion superconducting CeIrIn₅ thin films using the pulsed laser deposition (PLD) technique. X-ray diffraction study revealed that two types of thin films were grown, where TF1 is mainly a -axis oriented, while TF2 is the mixture of a - and c -axis orientation. Electrical resistivity measurements of both thin films showed a Kondo coherence peak and a zero-resistance phase transition, which are characteristics of heavy-fermion superconductivity. The temperature dependence of the upper critical field was similar to that of the bulk single crystal, indicating that the superconductivity of the thin film was similar to that of the bulk crystal. When subjected to the magnetic field, the temperature exponent n of the resistivity changes from 0.95 to 1.22 and 1.15 to 1.37 for TF1 and TF2, respectively, indicating the field-induced transition from the non-Fermi liquid regime toward the conventional Fermi-liquid regime.

II. EXPERIMENT

CeIrIn₅ thin films were deposited on MgF₂ (001) substrates using the PLD technique. The targets were prepared in-house by the arc melting method, wherein stoichiometric metal components (cerium 99.9%, iridium 99.95%, indium 99.999% purchased from Kojundo Chemical Lab) were melted together under an argon atmosphere. Contamination by oxygen was minimized using titanium metal as an oxygen absorber during the melting process. An excimer laser with a wavelength of 248 nm (LightMachinery IPEX-864) was used as a source to ablate the CeIrIn₅ polycrystalline target. Prior to the deposition, the MgF₂ (001) substrate was sequentially sonicated in acetone, ethanol, and diluted water. The base pressure of the PLD chamber was approximately

2.5×10^{-9} Torr and maintained at $\sim 10^{-8}$ Torr during deposition. Before deposition, the substrates were heated to 800 °C for 2 h to remove residual contamination on the surface. The total laser shot quantity and deposition temperature for TF1 and TF2 were 18,000 shots at 450 °C and 54,000 shots at 550 °C, respectively. The thicknesses of the films determined by field-emission scanning electron microscopy (FE-SEM) were 150 and 200 nm for TF1 and TF2, respectively. The crystal orientation of the thin films was verified using X-ray diffraction (XRD), and the lattice parameters were estimated using the FullProf software package. The thin films were categorized as TF1 and TF2 according to their crystal orientation. FE-SEM and energy-dispersive X-ray spectroscopy (EDX) were used to examine the thin-film surface morphology, thickness, and stoichiometry. Electrical transport measurements were performed using the standard four-probe technique in the temperature range of 0.3–300 K in the Physical Property Measurement System (PPMS), Oxford Teslatron, and ^3He -cryostat system (Oxford Heliox VL).

III. RESULTS AND DISCUSSION

Figures 1(a) and (b) show the XRD results for the CeIrIn_5 thin films of TF1 and TF2, respectively, deposited on the MgF_2 (001) substrate. For both films, CeIrIn_5 phase was observed with a small amount of impurity phases. In the case of TF1, the peaks ($h00$) of CeIrIn_5 phase were predominantly observed, revealing that the film grew along the a -axis. As shown in the SEM image (Fig. 1(c)), rectangular grains were formed in the TF1. However, the in-plane orientation of the rectangular layer (i.e., the ab or ac plane of CeIrIn_5) is not consistent with that of the MgF_2 substrate, indicating that the a -axis CeIrIn_5 layers were randomly oriented against the $[100]$ MgF_2 substrate. This type of grain has also been observed in c -axis-oriented CeCoIn_5 films on $c\text{-Al}_2\text{O}_3$ and MgO substrates grown using the PLD technique [14, 15]. In the case of TF2, both a -axis- and

c-axis-oriented grains were observed with additional peaks such as (101), (220), and (312) as shown in Fig. 1(b). XRD analysis showed that the *a*- and *c*-axis lattice constants for TF1 and TF2 were $a = 4.666 \text{ \AA}$ and $c = 7.523 \text{ \AA}$, and $a = 4.671 \text{ \AA}$ and $c = 7.513 \text{ \AA}$, respectively, as summarized in Table I. The lattice constant, *a*, of TF1 (TF2) was slightly reduced (expanded) compared with that of a single crystal, whereas the *c*-axis constant was expanded (reduced). The expansion of or reduction in the lattice constant in comparison with that of the single crystal may be ascribed to the strain induced by the substrate.

The surface morphologies of TF1 and TF2 obtained by FE-SEM are representatively displayed in Figs. 1(c) and (d), respectively. Rectangular grains were clearly observed for TF1, which could be assigned to CeIrIn₅ nanocrystals with an *a*-axis orientation. Smaller and randomly shaped domains were also observed in Fig. 1(c). The surface morphology of TF2, on the other hand, suggests that grains grew with vacant regions, which spread throughout the thin film. EDX analysis shows that the average stoichiometry for the rectangular region of TF1 and the layered region of TF2 was Ce: Ir: In = 1.12: 1.00: 4.57, whereas the stoichiometry outside the rectangular region of TF1 was Ce: Ir: In = 1.10: 1.00: 3.87, indicating that cerium is slightly in excess, whereas indium is deficient for all grains and boundaries.

In the case of TF1, when the ablated ionized atoms from the target reach the substrate surface at the early growth stage, they may not be adsorbed individually on the substrate; instead, the formation of *a*-axis CeIrIn₅ layers may facilitate the formation of rectangular layered structures. This type of growth is also observed in CeCoIn₅ nano/microcrystals on *r*-Al₂O₃ substrates and sometimes on MgF₂ substrates [16]. The residual adatoms, which cannot participate in the rectangular layer formation, form a randomly oriented CeIrIn₅ layer with indium deficiency. The relatively high indium deficiency may be due to its low boiling point. In the case of TF2, the entire

substrate was almost covered with layers, which could be associated with the increased substrate temperature and number of laser shots. The thicknesses measured from the cross-sectional FE-SEM images were approximately 150 nm and 200 nm for TF1 and TF2, respectively. The film thickness follows a linear relationship with the shot quantity, up to 18,000 shots. Afterward, the ablated atoms are consumed in forming the indium-deficient CeIrIn₅ layers with a higher yield, making full coverage of the layers on the substrate.

Figure 2(a) shows the normalized (divided by the 300 K value) electrical resistance for the TF1 and TF2 thin films and bulk single-crystal CeIrIn₅ [9]. The solid arrows mark the characteristic temperature with a local maximum—the coherence temperature (T_{coh}) below which conduction electrons coherently scatter off the lattice of Kondo singlets, reducing the resistance [17]. In contrast, for $T > T_{\text{coh}}$, the resistance followed a logarithmic temperature dependence, which is related to the incoherent scattering of the conduction electrons from Ce³⁺ local moments [18]. When compared with the bulk single crystal (~ 66 K), the thin-film T_{coh} values are shifted to lower temperatures of 41 and 37 K for TF1 and TF2, respectively.

Figure 2(b) shows the normalized resistance near the SC phase transition temperature (T_c), where the onset of T_c ($= T_{c,\text{on}}$) was decreased from 1.32 for bulk crystal to 0.58, and 0.52 K for TF1 and TF2 thin films, respectively. The width of the SC transition ΔT_c is 0.13 K for bulk crystal, while it is 0.29 and 0.20 K for TF1 and TF2 thin films, respectively. The residual resistivity ratio (RRR) estimated by $R(T = 300 \text{ K})/R(T_{c,\text{on}})$, as summarized in Table II, is significantly reduced from 46.8 for bulk crystal to 5.63 and 5.43 for TF1 and TF2 thin films, respectively, indicating that the increase in ΔT_c as well as the suppression in T_c is influenced by disorder in thin films [19].

The electrical resistances of TF1 and TF2 are plotted as a function of temperature near T_c for several magnetic fields applied along the MgF_2 [001] direction in Figs. 3(a) and (b), respectively. The dependence of $T_{c,on}$ on the magnetic field is plotted in Fig. 3(c), where the upper critical fields (H_{c2}) of TF1, TF2, and the single crystal for H applied perpendicular and parallel to the c -axis are described by black circles, red squares, blue up triangles, and green down triangles, respectively. The dashed lines represent the least-squares fittings of the phenomenological expression $H_{c2}(T) = H_{c2}(0)[1 - (T/T_{c,on})^2]^\beta$, where the fitting parameters are summarized in Table II. Figure 3(d) shows the scaling behavior of the reduced upper critical field ($H_{c2}/H_{c2}(T = 0 \text{ K})$) as a function of the reduced temperature (T/T_c ($\mu_0 H = 0 \text{ kOe}$)). All datasets of CeIrIn_5 thin films and single crystals are collapsed on top of each other where the value of β was 0.73 (see the red dash-dotted line), indicating that the nature of superconductivity in thin films is similar to that of bulk crystals.

Figures 4(a) and (b) show the electrical resistivity of TF1 and TF2, respectively, where 4 T (red circles) applied along the MgF_2 [001] direction was sufficient to suppress the SC phase. Similar to the bulk crystal, the resistance of thin films approximately followed the linear-in-T dependence: the temperature exponent (n) obtained from the least-square fits of $\rho(T) = \rho_0 + AT^n$ was 0.95 ± 0.01 and 1.15 ± 0.01 for TF1 and TF2, respectively. As the magnetic field was increased from 0 to 4 T, n increased from 0.95 to 1.22 and from 1.15 to 1.37 for TF1 and TF2, respectively. These results indicate that the non-Fermi liquid behavior observed at 0 T is associated with a quantum critical point (QCP), and the applied magnetic field drives the system away from the QCP [6, 21].

We note that the zero-resistance state of both TF1 and TF2 thin films is achieved at around 300 mK, which is significantly suppressed from that of the high- T_c phase ($T_c = 1.2 \text{ K}$), but is very

close to that determined from thermodynamic measurements. Lattice parameters determined from X-ray diffraction analysis (see Table I) indicate that both TF1 and TF2 films are under strain, possibly from the lattice mismatch with the substrate. The fact that both TF1 and TF2 shows lack of high- T_c phase seems at odds with the scenario that the high- T_c phase of CeIrIn₅ arises from the defect-strained patches. However, residual resistivity ratio (RRR) is 5.63 and 5.34 for TF1 and TF2 thin films, respectively, which is significantly lower than that of single crystalline sample (= 46.8), indicating that disorder is an important factor in determining the SC phase transition temperature. Further work on the growth of high-quality epitaxial thin film and the systematic control of disorder could be critical to properly understanding the mystery of the high- T_c phase in CeIrIn₅.

IV. CONCLUSION

In summary, we report the first successful deposition of CeIrIn₅ thin films on MgF₂ (001) substrates using the PLD technique. The coherence temperatures as well as the SC transition temperatures of the thin films were lower than the bulk single-crystal case, which could be related to the increase in the degree of disorder of the thin films. When plotted against the reduced temperature, the normalized upper critical fields of the thin films and bulk crystals were collapsed into a single curve, indicating that the nature of the superconductivity of thin films is similar to that of bulk single crystals. These results indicate that the PLD technique can be utilized as an alternative deposition method for the growth of heavy-fermion superconducting thin films. Further efforts to grow high-quality epitaxial thin films are expected to shed light on the evolution of the Kondo coherence behavior as well as unconventional superconductivity in the heavy-fermion superconductor family.

ACKNOWLEDGMENTS

This work was supported by a National Research Foundation (NRF) of Korea grant, funded by the Korean Ministry of Science and ICT (No. 2021R1A2C2010925). S Park, J. Kim, and J. –H. Kang were partially supported by the Basic Science Research Program through the National Research Foundation of Korea (NRF), funded by the Ministry of Education (NRF-2016R1A6A3A11935214 and NRF-2018R1D1A1B07051040). W. S. Choi was supported by NRF- 2021R1A2C2011340.

REFERENCES

- [1] Tuson Park, F. Ronning, H. Yuan, M. B. Salamon, R. Movshovich, J. L. Sarrao, and J. D. Thompson, Hidden Magnetism and Quantum Criticality in the Heavy Fermion Superconductor CeRhIn₅, *Nature* **440**, 65 (2006).
- [2] Tuson Park, V. A. Sidorov, F. Ronning, J.-X. Zhu, H. Lee, E. D. Bauer, R. Movshovich, J. L. Sarro, and J. D. Thompson, Isotropic quantum scattering and unconventional superconductivity, *Nature* **456**, 366 (2008).
- [3] M. Kenzelmann, Th. Strässle, C. Niedermayer, M. Sigrist, B. Padmanabhan, M. Zolliker, A. D. Bianchi, R. Movshovich, E. D. Bauer, J. L. Sarrao, and J. D. Thompson, Coupled Superconducting and Magnetic Order in CeCoIn₅, *Science* **321**, 1652 (2008).
- [4] P. Monthoux, D. Pines, and G. G. Lonzarich, Superconductivity without phonons, *Nature* **450**, 1177 (2007).
- [5] Soon-Gil Jung, Soonbeom Seo, Sangyun Lee, Eric D. Bauer, Han-Oh Lee, and Tuson Park, A peak in the critical current for quantum critical superconductors, *Nat. Commun.* **9**, 434 (2018).
- [6] Johnpierre Paglione, M. A. Tanatar, D.G. Hawthorn, Etienne Boaknin, R.W. Hill, F. Ronning, M. Sutherland, and Louis Taillefer, C. Petrovic, and P.C. Canfield, Field-Induced Quantum Critical Point in CeCoIn₅, *Phys. Rev. Lett.* **91**, 246405 (2003).
- [7] Y. Mizukami, H. Shishido, T. Shibauchi, M. Shimozawa, S. Yasumoto, D. Watanabe, M. Yamashita, H. Ikeda, T. Terashima, H. Kontani, and Y. Matsuda, Extremely strong-coupling superconductivity in artificial two-dimensional Kondo lattices, *Nat. Phys.* **7**, 849 (2011).
- [8] T. Ishii, R. Toda, Y. Hanaoka, Y. Tokiwa, M. Shimozawa, Y. Kasahara, R. Endo, T. Terashima, A. H. Nevidomskyy, T. Shibauchi, and Y. Matsuda, Tuning the Magnetic Quantum Criticality of Artificial Kondo Superlattices CeRhIn₅/YbRhIn₅, *Phys. Rev. Lett.* **116**, 206401 (2016).

- [9] C. Petrovic, R. Movshovich, M. Jaime, P. G. Pagliuso, M. F. Hundley, J. L. Sarrao, Z. Fisk, and J. D. Thompson, A new heavy-fermion superconductor CeIrIn₅: A relative of the cuprates?, *Europhys. Lett.*, **53**, 354 (2001).
- [10] R. Movshovich, M. Jaime, J. D. Thompson, C. Petrovic, Z. Fisk, P. G. Pagliuso, and J. L. Sarrao, Unconventional Superconductivity in CeIrIn₅ and CeCoIn₅: Specific Heat and Thermal Conductivity Studies, *Phys. Rev. Lett.* **86**, 5152 (2001).
- [11] G.-q. Zheng, K. Tanabe, T. Mito, S. Kawasaki, Y. Kitaoka, D. Aoki, Y. Haga, and Y. Onuki, Unique Spin Dynamics and Unconventional Superconductivity in the Layered Heavy Fermion Compound CeIrIn₅: NQR Evidence, *Phys. Rev. Lett.* **86**, 4664 (2001).
- [12] Maja D. Bachmann, G. M. Ferguson, Florian Theuss, Tobias Meng, Carsten Putzke, Toni Helm, K. R. Shirer, You-Sheng Li, K. A. Modic, Michael Nicklas, Markus König, D. Low, Sayak Ghosh, Andrew P. Mackenzie, Frank Arnold, Elena Hassinger, Ross D. McDonald, Laurel E. Winter, Eric D. Bauer, Filip Ronning, B. J. Ramshaw, Katja C. Nowack, and Philip J. W. Moll, Spatial control of heavy-fermion superconductivity in CeIrIn₅, *Science*, **366**, 221 (2019).
- [13] Masaaki Shimozawa, Swee K Goh, Takasada Shibauchi, and Yuji Matsuda, From Kondo lattices to Kondo superlattices, *Rep. Prog. Phys.* **79** 074503 (2016).
- [14] Jihyun Kim, Hanul Lee, Sangyun Lee, Sungmin Park, Tuson Park, YoonHee Cho, Hyoyoung Lee, Won Nam Kang, and Woo Seok Choi, Synthesis of heavy fermion CeCoIn₅ thin film via pulsed laser deposition, *Curr. Appl. Phys.* **19**, 1338 (2019).
- [15] Jens Hänisch, Filip Ronning, Roman Movshovich, and Vladimir Matias, Pulsed laser deposition of CeCoIn₅ thin films, *Physica C*, **470**, S568 (2010).
- [16] CeCoIn₅ nano/micro islands have been formed on *r*-Al₂O₃ and MgF₂ substrate with our PLD system, and the island has been found to be *c*-axis oriented. These data are not included in this article.
- [17] Piers Coleman, arXiv:1509.05769v1 (2015).
- [18] Sooyoung Jang, J. D. Denlinger, J. W. Allen, V. S. Zapf, M. B. Maple, Jae Nyeong Kim, Bo Gyu Jang, and Ji Hoon Shim, Evolution of the Kondo lattice electronic structure above the transport coherence temperature, *PNAS*, **117**, 23467 (2020).
- [19] J. Paglione, T. A. Sayles, P.-C. Ho, J. R. Jeffries, and M. B. Maple, Incoherent non-Fermi-liquid scattering in a Kondo lattice, *Nat. Phys.* **3**, 703 (2007).

- [20] Hiroaki Shishido, Rikio Settai, Dai Aoki, Shugo Ikeda, Hirokazu Nakawaki, Noriko Nakamura, Tomoya Iizuka, Yoshihiko Inada, Kiyohiro Sugiyama, Tetsuya Takeuchi, Kouichi Kindo, Tatsuo C. Kobayashi, Yoshinori Haga, Hisatomo Harima, Yuji Aoki, Takahiro Namiki, Hideyuki Sato, and Yoshichika Ōnuki, Fermi Surface, Magnetic and Superconducting Properties of LaRhIn₅ and CeTIn₅ (T: Co, Rh and Ir), *J. Phys. Soc. Jpn.* **71**, 162 (2002).
- [21] A. Bianchi, R. Movshovich, I. Vekhter, P.G. Pagliuso, and J. L. Sarrao, Avoided Antiferromagnetic Order and Quantum Critical Point in CeCoIn₅, *Phys. Rev. Lett.* **91**, 257001 (2003).

FIGURES

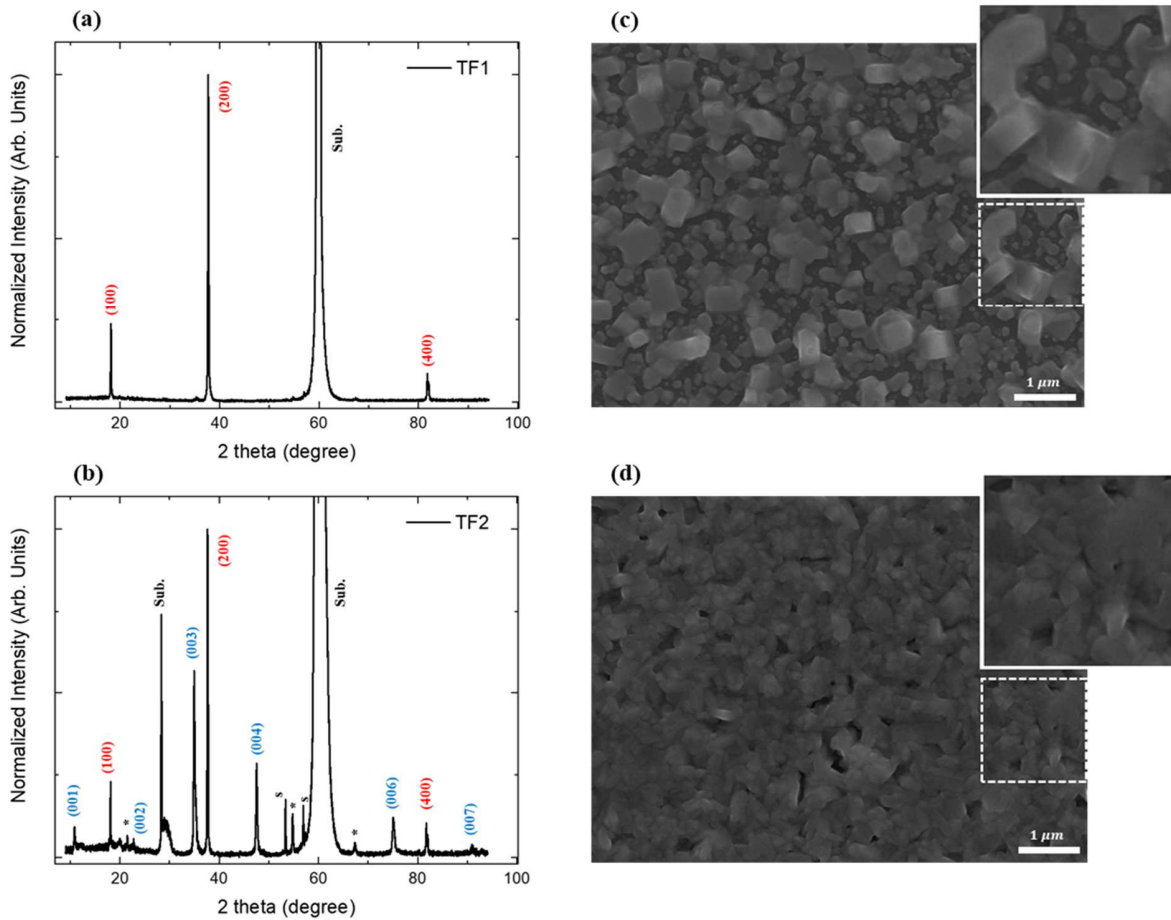


FIG. 1. X-ray diffraction and FE-SEM results of TF1 and TF2 deposited on a MgF_2 (001) substrate. The a - and c -axis orientations of TF1 and TF2 are denoted by the red and blue miller indices in (a) and (b), respectively. TF1 shows mainly a -axis oriented thin-film growth, whereas TF2 shows biaxial (combination of a - and c -axis orientation) growth. The different surface morphologies of TF1 and TF2, which were probed by FE-SEM, are shown in (c) and (d), respectively. The inset in the SEM displays the magnified image of the region indicated by the white dotted square. The thickness was measured to be 150 and 200 nm for TF1 and TF2, respectively.

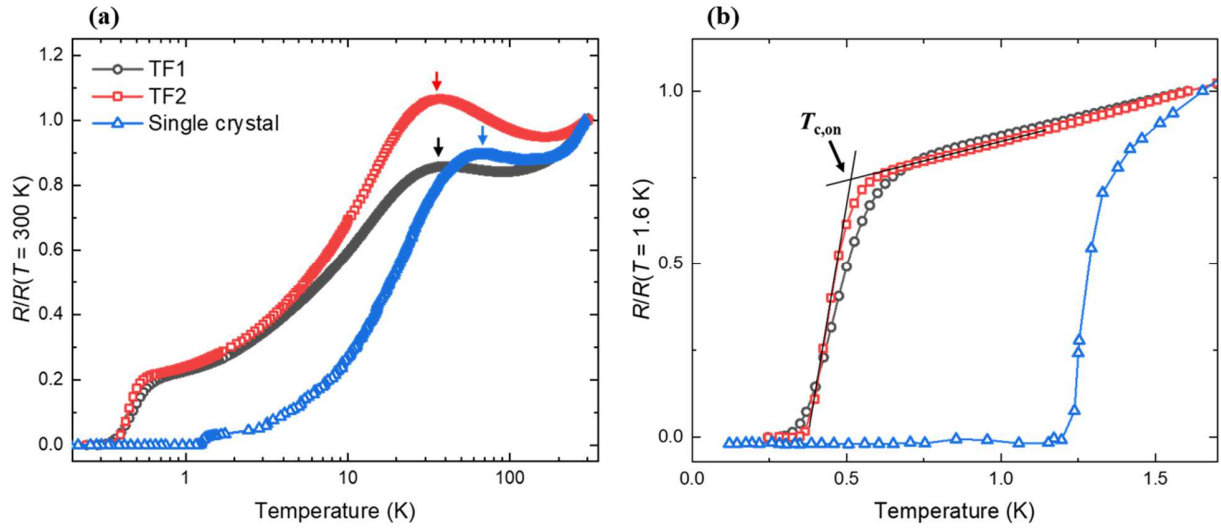


FIG. 2. (a) Electrical resistances of TF1, TF2, and bulk crystal, which are normalized by the resistance at 300 K, are plotted as a function of temperature. Solid arrows mark the coherence temperature (T_{coh}), where the resistance reveals a peak. (b) Electrical resistance is magnified near the SC phase transition. When compared with the bulk crystal, the onset temperatures of SC transition ($T_{\text{c,on}}$) of the thin films were suppressed. The arrow marks the criteria for the $T_{\text{c,on}}$ of this study.

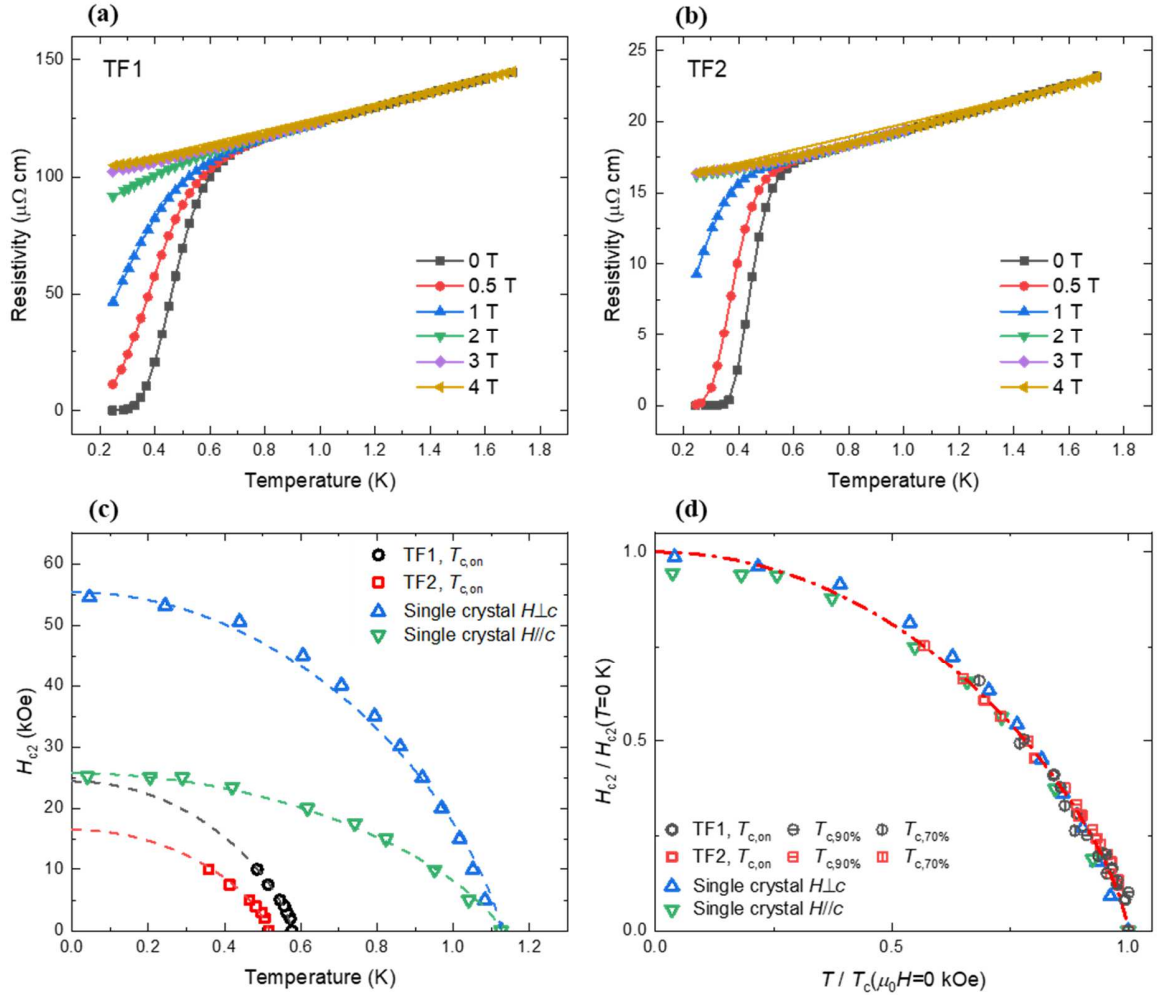


FIG. 3. Electrical resistances of TF1 and TF2 are plotted against temperature for several magnetic field in (a) and (b), respectively. (c) The upper critical field determined from $T_{c,on}$ is plotted as a function of temperature for TF1 (black circles), TF2 (red squares), and bulk single crystal for $H_{\perp}c$ (blue up triangles) and $H_{\parallel}c$ (green down triangles). The dashed lines are the best results obtained from the least-squares fittings of the phenomenological expression $H_{c2}(T) = H_{c2}(0)[1 - (T/T_{c,on})^2]^\beta$. (d) Reduced upper critical field as a function of reduced temperature for CeIrIn₅ single crystals and thin films. Upper critical fields determined from $T_{c,90\%}$ and $T_{c,70\%}$ are additionally plotted. The scaling behavior (red dash-dotted line) showed that the temperature dependence of the reduced upper critical field was independent of the criterion used to determine T_c .

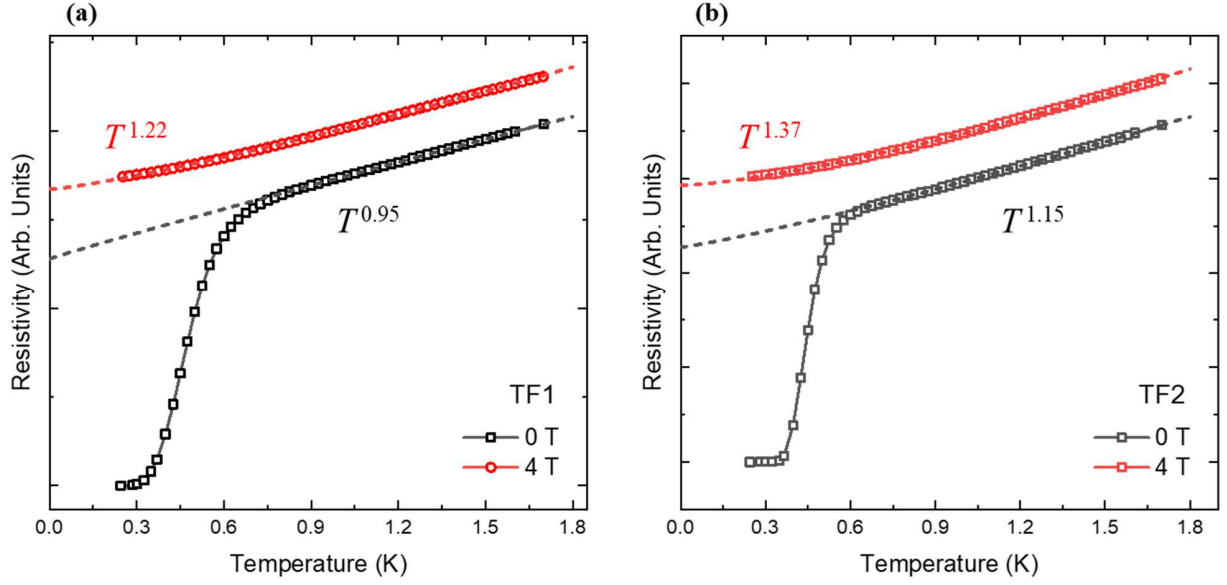


FIG. 4. Temperature dependence of resistance under magnetic fields of 0 (black squares) and 4 T (red circles) for (a) TF1 and (b) TF2. The 4 T resistivity curve is shifted for clarity. The dashed lines show best results from the least-squares fitting of $\rho(T) = \rho_0 + AT^n$. The temperature exponent of the CeIrIn₅ thin films increased with application of magnetic field.

TABLE I. Summary of the surface morphology and structural properties of single-crystal and thin-film CeIrIn₅.

	Morphology	a (Å)	c (Å)	c/a
Single Crystal ^a		4.668	7.515	1.610
TF1	Island	4.666 (-0.043%)	7.523 (+0.106%)	1.612
TF2	Grained Layer	4.671 (+0.064%)	7.513 (-0.027%)	1.608

^a Reference [9]

TABLE II. Summary of superconducting transition temperature, upper critical field (fitting parameter), coherence temperature, and residual resistivity ratio (RRR) of single crystal and thin-film CeIrIn₅.

	$T_{c,on}$ (K)	$T_{c,zero}$ (K)	ΔT_c (K)	$H_{c2}(0)$ (kOe) (β)	T_{coh} (K)	RRR
Single Crystal ^a	1.32	1.19	0.13	$(H \perp c)$ 55.4 (0.735) $(H // c)$ 25.7 (0.737)	66.6	46.8
TF1	0.58	0.29	0.29	24.4 (0.712)	40.9	5.63
TF2	0.52	0.32	0.20	16.5 (0.708)	36.9	5.43

^a Reference [20]